Lattice expansion and noncollinear to collinear ferrimagnetic order in a $MnCr_2O_4$ nanoparticle

R. N. Bhowmik* and R. Ranganathan†
Experimental Condensed Matter Physics Division, Saha Institute of Nuclear Physics, Kolkata 700064, India

R. Nagarajan
Condensed Matter Physics Division, Tata Institute of Fundamental Research, Colaba Road, Mumbai, India
(Received 21 January 2005; revised manuscript received 28 November 2005; published 12 April 2006)

We report the magnetic behavior of spinel chromite $MnCr_2O_4$. Bulk $MnCr_2O_4$ shows a sequence of magnetic states, i.e., paramagnetic (PM) to collinear ferrimagnetic (FM) state below $T_C \sim 45$ K and collinear FM state to noncollinear FM state below $T_S \sim 18$ K. Decrease of particle size reduces the noncollinear spin structure and consequently, magnetic transition at T_S decreases in nanoparticle samples. However, ferrimagnetic order is still dominating in nanoparticles, except the observation of superparamagnetic-like blocking and decrease of spontaneous magnetization. This, according to the core-shell model of ferrimagnetic nanoparticles, may be due to surface disorder effects of nanoparticles. The system also shows the increase of T_C in nanoparticle samples, which is not consistent with the core-shell model. The analysis of the $M(T)$ data, applying spin wave theory, has shown an unusual Bloch exponent value 3.35 for bulk $MnCr_2O_4$, which decreases and approaches 1.5, a typical value for any standard ferromagnet, with decreasing particle size. We have also observed the lattice expansion in $MnCr_2O_4$ nanoparticles. The present work shows the correlation between a systematic increase of lattice parameter and the gradual decrease of B site noncollinear spin structure in $MnCr_2O_4$.

DOI: 10.1103/PhysRevB.73.144413 PACS number(s): 75.75.+a, 81.20.Ev

I. INTRODUCTION

Spinel ferrite,[1] represented by formula unit AB_2X_4, has generated renewed research interest due to applications in nanoscience and technology. It has been established that the physical properties of spinel ferrites depend upon the distribution of cations among the tetrahedral (A) and octahedral (B) sites and relative strengths of superexchange interactions via anions (X=O,S,Se ions). It is noted that most of the works are confined on spinel ferrites MFe_2O_4 (M=Zn,Co, Mn,Ni, etc.).[2] In these spinels B sites are occupied by Fe^{3+}. There are many spinels of different class and having no B site Fe^{3+}, but which may be very relevant in view of physics and technological applications. Chromites MCr_2X_4 (M=Mn, Fe, etc., X=O,S ions) are one of such classes which exhibit many unusual magnetic properties like ferrimagnetism, colossal magnetoresistance (CMR) effect, etc. Recently, extensive work on half-metallic ferrimagnet (HFM) $FeCr_2S_4$ shows interesting magnetic properties with different (magnetic and nonmagnetic) substitutions.[3–5] It has been proposed[4] that $Mn[Cr_{2-x}V_x]S_4$ series might be a strong candidate for HFM. One would expect similar magnetic and transport properties in MCr_2O_4 in comparison with MCr_2S_4, since both (sulfide and oxide) spinels have identical cubic lattice structure, and both are ferrimagnet with T_C in the range 60–80 K and noncollinear ferrimagnet below 20 K. The other interest for investigating the $MnCr_2O_4$ spinel is to understand the role of strongly negative J_{BB} (Cr-O-Cr) interactions in controlling the magnetic properties of chromites. In collinear ferrimagnetic structure of spinel A-O-B and B-O-B bond angles are 125° and 90°, respectively. For other configurations the distance between the oxygen ion and cations are too large to give rise to a strong A-O-B superexchange interaction. The investigation of the magnetic properties of chromites[6] revealed a number of unconventional features which could not be explained by Neel's theory for collinear (ferrimagnetic) spin structure.

Wickham and Goodenough[6] have proposed that direct (antiferromagnetic) interactions between B site cations are responsible for the noncollinear ferrimagnetic structure in chromites like $MnCr_2O_4$. In fact, many phenomena in recent years have been explained in terms of B site direct cation-cation interaction, as in $ZnCr_2O_4$.[7] Neutron diffraction experiment confirmed the noncollinear spin structure between B site Cr^{3+} moments in chromites,[8] including $MnCr_2O_4$.[9] The neutron experiment shows that the decrease of magnetization in $MnCr_2O_4$ below 18 K, though identical with reentrant magnetic transition,[10] originates from the occurring of noncollinear spin structure in $MnCr_2O_4$.

Numerous attempts have been made to bridge the gap between ferrites (MFe_2O_4), which are collinear ferrimagnet, and chromites, which are noncollinear ferrimagnet. However, the picture of spin configuration of chromites is still not clear.[11] The present work highlights the magnetic ordering in bulk and nanoparticles of $MnCr_2O_4$ chromite with a focus to understand the origin of magnetic transition at ~18 K in $MnCr_2O_4$.

II. EXPERIMENTAL RESULTS

A. Sample preparation and characterization

We have prepared $MnCr_2O_4$ nanoparticles by mechanical milling of the bulk material using Fritsch Planetary Mono Mill "Pulverisette 6." The bulk $MnCr_2O_4$ sample was prepared with the stoichiometric mixture of MnO (99.999% purity) and Cr_2O_3 (99.997% purity) oxides. The mixture was grounded for 2 h and pelletized. The pellet was sintered at

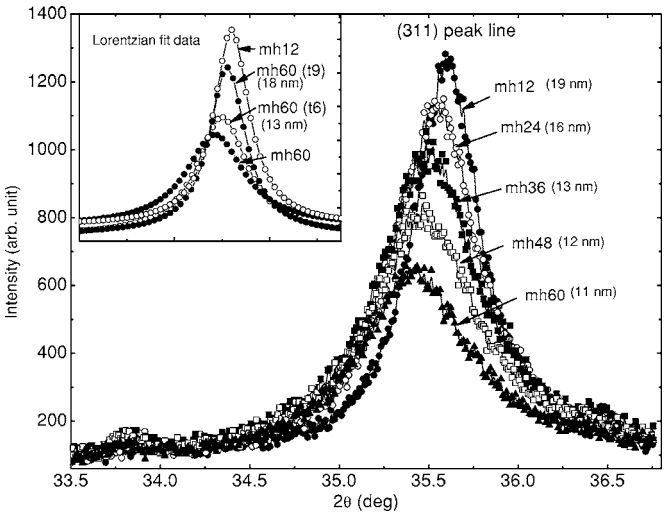

FIG. 1. Variation of (311) XRD peak line of cubic spinel structure with milling hours and the same (311) line is compared with the mh60 sample after annealing at 600 °C [mh60($t6$)] and 900 °C [mh60($t9$)] for 12 h.

1000 °C for 12 h and at 1200 °C for 24 h with intermediate grinding. The sample was then cooled to room temperature at 2 to 3 °C/min. The bulk sample was grounded for 2 h before milling. X-ray diffraction (XRD) spectra of the bulk sample was recorded using a Philips PW1710 diffractometer with Cu $K\alpha$ radiation. The XRD spectra of bulk sample matched with a typical spinel structure in cubic phase. The powdered $MnCr_2O_4$ (bulk) material was mechanical milled in a 80 ml agate vial with 10 mm agate balls with ball-to-sample mass ratio 12:1. The sintering and milling of bulk sample was carried out in argon atmosphere to prevent the oxidation of Mn^{2+}. The milled samples are designated as mh$X$, where X denotes the number of milling hours. The XRD spectra of milled samples are also matched with standard cubic spinel structure. The XRD spectrum, without any additional phase, shows that both bulk and nanoparticle samples are single phase chromites and have identical chemical composition. The absence of any impurity lines excludes the possibility of the formation of other alloyed compounds during mechanical milling. The lattice parameters of the samples were determined by standard full profile fitting method (Rietveld method) using the FULLPROF program. The calculations were performed assuming that the samples belong to $Fd3m$ space group and ascribed to normal cubic spinel structure. The XRD peak lines were fitted with Lorentzian shape. The lattice parameter of our bulk sample is 8.41(±0.002) Å, which is close enough to the reported value 8.42(±0.02) Å (Ref. 12) and 8.437 Å.[13] The systematic broadening of XRD lines (Fig. 1) with milling time corresponds to the decrease of particle size (Table I). The particle size was determined from the analysis of XRD 311 line using the Debye-Scherrer equation. The effect of microstrain, induced in the material during milling, in the determination of half-width has been minimized by matching the 311 line of the XRD spectra with Lorentzian shape. We have taken TEM data for three samples, i.e., mh60, mh48, and mh36. The TEM pictures (Fig. 2) show that the samples have small distribution in particle size. The TEM data, shown in Fig. 2, give average particle size ~12, 13, and 15 nm in comparison with XRD data 11, 12, and 13 nm for samples mh60, mh48, and mh36, respectively. This shows that the effect of mechanical strain is not significant in our determination of particle size using XRD data. It is found (Table I) that the lattice parameter of the system systematically increases with the decrease of particle size. This is reflected in the shift of the XRD peaks, as shown for the 311 line in Fig. 1, to lower scattering angle (2θ) with increasing milling time. We, further, examined the origin of the shift of XRD peak with decreasing particle size by annealing the mh60 sample at

TABLE I. The parameters for milled sample mh$X$, where X represents milling time in hours on bulk sample. Particle size (D) and lattice parameter a (Å) were obtained from XRD spectra. Saturation magnetization at 0 K (M_0) was obtained from the $M(T)$ data at 50 kOe. T_C was determined from first order derivative of $M(T)$, M_S (T), and ac susceptibility data.

Sample	D (nm)	a (±0.002 Å)	T_C (K)	M_0 (emu/g)
mh0	150	8.410	44±1	30.54
mh12	19	8.412	46±1	25.91
mh24	16	8.425	47±1	25.24
mh36	13	8.440	49±1	22.81
mh48	12	8.448	51±1	22.35
mh60	11	8.474	52±1	21.78

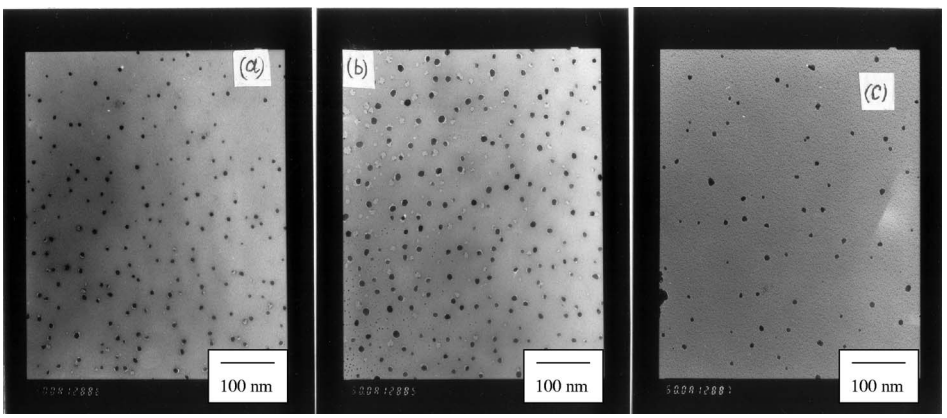

FIG. 2. TEM data for samples (a) mh60 of particle size ~12 nm, (b) mh48 of particle size 13 nm, and (c) mh36 of particle size 15 nm.

600 °C [denoted as mh60(t6)] and 900 °C [denoted as mh60(t9)] for 12 h under vacuum sealed condition. We have seen (inset of Fig. 1) that the 311 peak of the annealed sample tends toward the bulk sample. The decrease of lattice parameter, e.g., 8.474 Å (for mh60, particle size ~11 nm), 8.442 Å [for mh60(t6), particle size ~13 nm], 8.424 Å [for mh60(t9), particle size ~18 nm], and 8.410 Å (for bulk sample), with increasing annealing temperature (i.e., increase of particle size) confirm the lattice expansion in our nanoparticles.

B. dc magnetization

1. Temperature dependence of magnetization

The temperature dependence of dc magnetization (Fig. 3) was measured under zero field cooled (ZFC) and field cooled (FC) modes, using a superconducting quantum interference device (SQUID) (Quantum Design) magnetometer. In ZFC mode, the sample was cooled from 300 to 2 K in the absence of dc magnetic field, followed by the application of magnetic field at 2 K and magnetization data were recorded while increasing the temperature. In FC mode, the sample was cooled from 300 K in the presence of field. In FC mode cooling field and measurement fields are the same. The zero field cooled magnetization (MZFC) at 100 Oe of bulk sample [Fig. 3(a)] shows an increase below 45 K and remains almost temperature independent in the temperature range 40–18 K. Below 18 K, MZFC sharply decreases down to our measurement temperature 2 K. The magnetic behavior of our bulk $MnCr_2O_4$ is consistent with the reported[11,14] data, where paramagnetic to ferrimagnetic transition occurs below $T_C \approx 45$ K and collinear spin structure in B sites becomes noncollinear (canted) below $T_S \approx 18$ K due to the dominance of J_{BB} interactions over J_{AB} interactions.[13] There is a small magnetic irreversibility (MFC > MZFC) between field cooled magnetization (MFC) and MZFC below 40 K. The magnetic change observed in MZFC at $T_S \approx 18$ K also exists in MFC. It is noted that T_S remains almost unchanged up to field ~1 kOe, but gets suppressed at 50 kOe data. This is consistent with a strong noncollinear ferrimagnetic order in bulk sample below 18 K, and such magnetic order is affected only at high magnetic field.

The $M(T)$ (MZFC and MFC) data for nanoparticle (mh12, mh24, mh36, mh48, and mh60) samples are shown in Figs. 3(b)–3(f). The behavior is different in comparison with the bulk. For example, magnetic irreversibility between MZFC and MFC starts above 45 K and the separation between MZFC and MFC increases on lowering the temperature. The other important observation is that plateau behavior in the magnetization data (temperature range 40–18 K) of the bulk sample slowly decreases and a maximum occurs below 40 K with decreasing the particle size [Fig. 3(f)]. Note that there is no decrease of MFC below 18 K, instead the MFC in all nanoparticle samples shows continuous increase down to 2 K. Figure 3(f) (for mh60 sample) shows that the temperature T_{irr}, where magnetic irreversibility starts, decreases with increase of magnetic field. This behavior of $M(T)$ data along with a large difference in MFC and MZFC shows blocking phenomenon of ferrimagnetic nanoparticles.[15] We now analyze the $M(T)$ data to understand the particle size effect. Figure 4(a) shows the temperature dependence of the inverse of dc magnetic susceptibility (χ), using MZFC data at 100 Oe. It is interesting to note that $\chi^{-1}(T)$ of bulk and nanoparticle samples follow the typical functional form: $\chi^{-1} = T/C + 1/\chi_0 - \sigma/(T-\theta)$, which consists of a Curie-Weiss (ferromagnetic) term and a Curie (paramagnetic) term and such an equation has shown its application in ferrimagnetic spinel.[16] This means strong ferrimagnetic order still exists in our nanoparticles. The estimation of the constants C and σ from this equation is difficult because they are coupled in the paramagnetic regime. The asymptotic Curie temperature (θ), obtained by extrapolation, is shown in the inset of Fig. 4. The closeness of T_C and θ in bulk sample characterizes its long range ferrimagnetic order. On the other hand, θ values for nanoparticle sample (e.g., ~60 K for particle size ~19 nm,

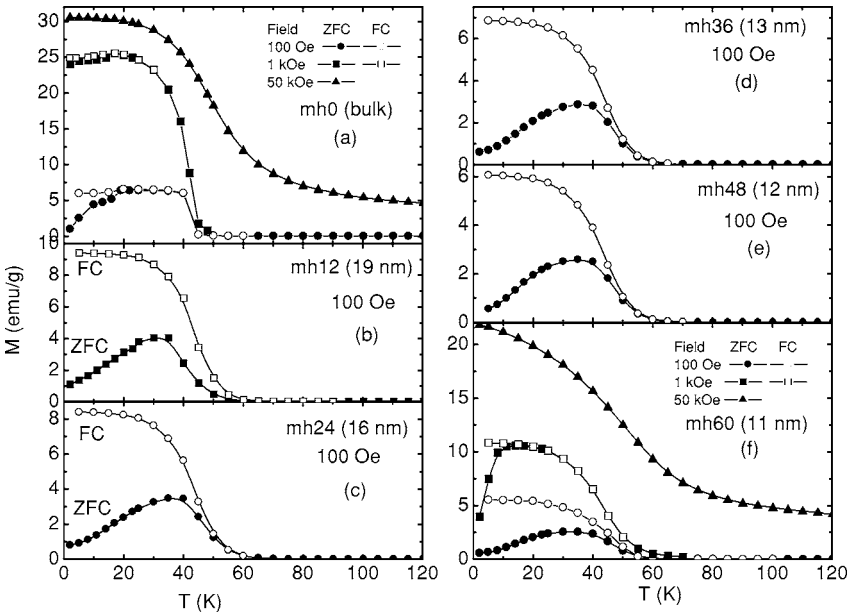

FIG. 3. Temperature dependence of magnetization at different magnetic fields for bulk and mechanical milled nanoparticle samples. Solid symbols and open symbols represent MZFC and MFC data, respectively.

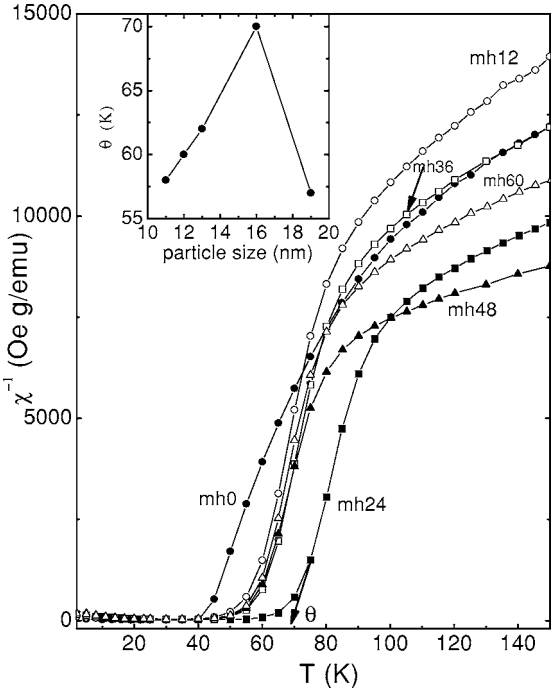

FIG. 4. χ^{-1} vs T data at measurement field 100 Oe for bulk and nanoparticle (mh$X$) samples. θ indicates asymptotic Curie temperature. The inset shows particle size (mh0: bulk, mh12: 19 nm, mh24: 16 nm, mh36: 13 nm, mh48: 12 nm, and mh60: 11 nm) dependence of θ.

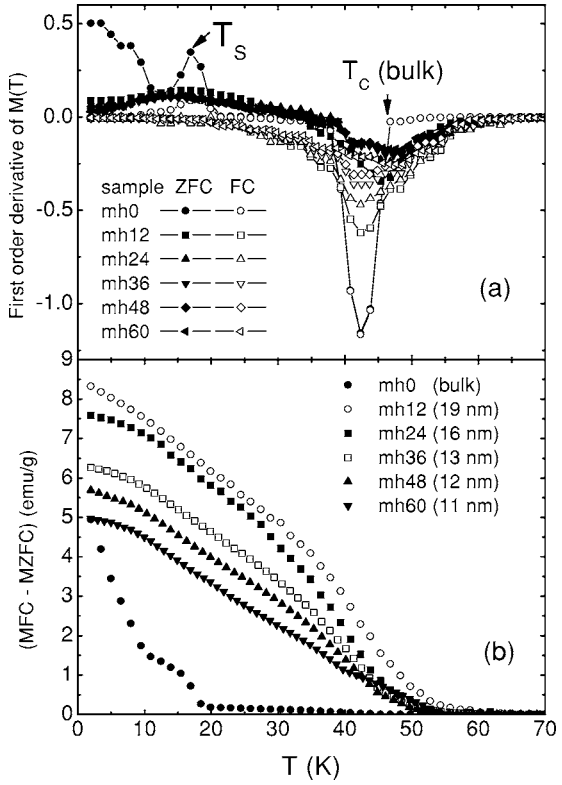

FIG. 5. (a) First order derivative of $M(T)$ vs temperature. (b) TRM (MFC−MZFC) vs temperature for bulk and nanoparticle samples. Measurement field is 100 Oe.

~70 K for particle size ~16 nm) are much higher than the θ~45 K for bulk. The increasing magnetic disorder in nanoparticle is manifested by the large difference between θ and T_C,[17] and broadening of the change in magnetization with temperature about T_C. According to the core-shell model of ferrimagnetic nanoparticles,[18] the disorder is associated with increasing contribution of shell (surface) spins and long range ferrimagnetic order is associated with core spins.

From the first order derivative of $M(T)$ (both ZFC and FC) data [Fig. 5(a)], we find that there is a minimum below T_C (~45 K) for bulk sample. This minimum for MZFC becomes broad for nanoparticle samples occurring at higher temperature with respect to the bulk sample. The increasing broadness about the minimum is related to the disorder effects in nanoparticle samples. This is understood from the fact that the sample is magnetically more ordered in the FC state than the ZFC state. The first order derivative of $M(T)$ [Fig. 5(a)] shows a sharp peak near T_S~18 K for bulk sample, which is broadened for nanoparticle samples. This indicates that B site (noncollinear) spin configuration below 18 K has been changed in nanoparticles. The difference between field cooled magnetization and zero field cooled magnetization (ΔM=MFC−MZFC) vs T data [Fig. 5(b)] show that for bulk sample the ΔM is very small in the temperature range 40–18 K and increases below 18 K. For nanoparticle samples, ΔM shows significant increase below 60 K with shape different from the bulk. The large magnitude of ΔM over the whole temperature range, comparing the bulk sample, suggests increasing disorder effects in nanoparticle samples. On the other hand, shifting of the MZFC minimum of nanoparticle samples to higher temperature may indicate the increase of T_C with decreasing the particle size. Due to the increasing flatness about 45 K in $M(T)$ data and occurrence of separation between MFC and MZFC well above 45 K, it is very difficult to estimate the exact T_C values for nanoparticle samples. The spin wave theory can be applied, since ferrimagnetic order dominates in both bulk and nanoparticle samples. We have analyzed the MZFC data at 50 kOe [Fig. 6(a)], using the Bloch law: $M(T)=M_0(1-\beta T^{\alpha})$. Here, M_0 is the extrapolated value of saturation magnetization at 0 K, and β and α are the constants. The change of M_0, Bloch exponent α, and Bloch coefficient β with particle size are shown in Table I, and in Fig. 6(b), respectively. The saturation magnetic moment ~30 emu/g [or magnetic moment ~1.46 (±0.01)μ_B per formula unit] at 2 K of our bulk sample is consistent with the reported value 1.4–1.6 μ_B.[6] It is interesting from the log-log plot of $[M_0-M(T)]$ vs T [Fig. 6(a)] that curves for all the samples intersect at the same temperature point ~44 K. This observation is notable in the sense that this temperature point is close to the T_C~45 K of the bulk sample and invariant with particle size down to ~11 nm. The Bloch exponent $\alpha=3.35\pm0.04$ for bulk $MnCr_2O_4$ is large in comparison with $\alpha=1.5$ for a typical ferromagnet.[19] The exponent is reducing and approaching to the typical value of 1.5 with the decrease of particle size. For example, $\alpha=1.7\pm0.05$ for sample of particle size ~11 nm. The theoretical calculation, as well as some experimental results on fine particles and clusters,[20,21] have shown that α becomes larger than 1.5, the value corre-

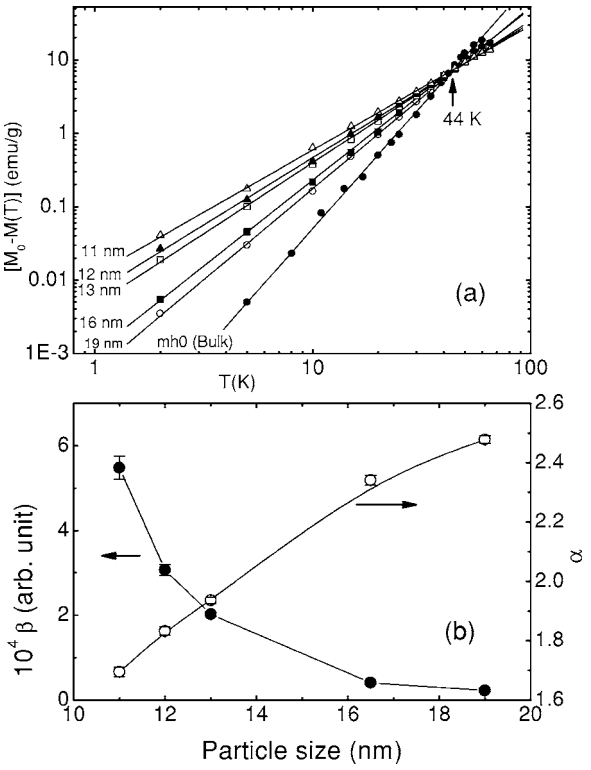

FIG. 6. (a) log-log plot of $[M_0-M(T)]$ vs T for MZFC at 50 kOe data. M_0 for each sample was estimated by extrapolating the MZFC data to 0 K. (b) Particle size dependence of the exponents obtained from Bloch law. For bulk sample α is 3.35 (not shown in the figure).

sponding to bulk material. Hence the particle size dependence of α is unconventional in $MnCr_2O_4$, where α decreases with decrease of particle size. The feature is that $T^{3/2}$ spin wave law alone cannot be applied for bulk sample and there is a possibility of another origin contributing in $M(T)$ behavior. The extra magnetic contributions may introduce from a modulated magnetic order, arising from the noncollinear spin structure[22] in bulk system or alternation of core-shell structure[23] in nanoparticles. The tendency of decreasing the exponent towards 1.5, a typical value for standard ferro- or ferrimagnet, for smaller particles suggests that the extra magnetic contribution, introduced due to the noncollinear structure of B site spins, decreases with the decrease of particle size.

2. Field dependence of magnetization

Figures 7(a)–7(c) show the $M(H)$ data and Figs. 7(d) and 7(e) show the corresponding Arrot plot (M^2 vs H/M) for bulk (mh0), mh60, and mh48 samples, respectively. In bulk sample, an initial increase of M to its spontaneous magnetization (M_S) value within 1 kOe is followed by the lack of saturation with field (H) up to 120 kOe, for all temperatures below T_C. For higher temperatures, e.g., $T=40$ and 50 K, the nonlinear contribution of $M(H)$ is increasing in our bulk sample. Similar $M(H)$ behavior in $MnCr_2S_4$ (Ref. 8) has been attributed to the coexistence of ferrimagnetic state and quasiparamagnetic state, arising from the noncollinear spin structure. The noncollinear spin structure between B site Cr^{3+} moments $MnCr_2O_4$ has been confirmed by neutron diffraction experiment.[9] The nonsaturation of magnetization at higher field is attributed to paramagnetic type contributions, as shown in the inset of Fig. 7(a), arising from the B site noncollinear spin structure. The nonlinear contribution in $M(H)$ data is observed even at lower temperatures for nanoparticle samples, as shown in Fig. 7(b) for the mh60 sample. Figure 7(c) suggests that a typical paramagnetic state [the linear increase of $M(H)$] for the mh48 sample is observed only above 70 K. The gradual change in $M(H)$ data near T_C and above makes it difficult to determine the exact value of T_C. In order to distinguish the long range order ferrimagnetic state from the paramagnetic state, we have analyzed the $M(H)$ data using Arrot plot (M^2 vs H/M). The Arrot plots are shown in Figs. 7(d)–7(f). We have calculated the magnitude of spontaneous magnetization (M_S) by extrapolating the data for $H \geq 10$ kOe to the M^2 axis. Although $M(H)$ data at

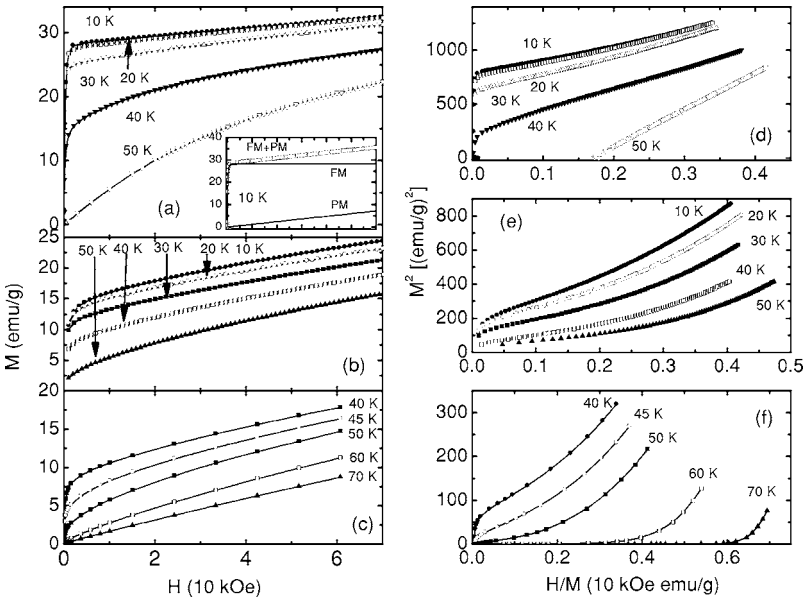

FIG. 7. Field dependence of magnetization at selected temperatures for samples (a) mh0 (bulk), (b) mh60 (11 nm), and (c) mh48 (12 nm), and corresponding Arrot plots (M^2 vs H/M) for samples (d) mh0, (e) mh60, and (f) mh48. Inset of (a) shows the $M(H)$ data at 10 K for bulk sample with field 0–120 kOe.

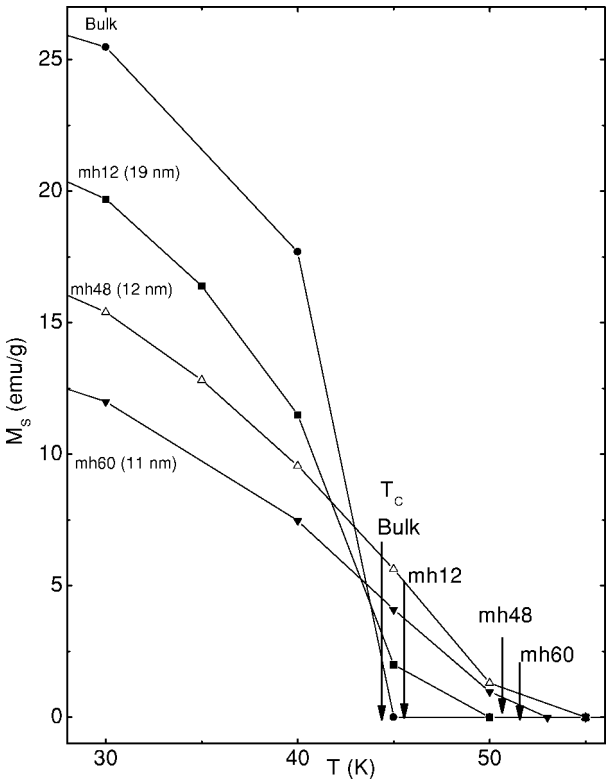

FIG. 8. Temperature dependence of M_S, derived from Arrot plot, to estimate the temperatures (T_C) at which M_S becomes zero.

50 K [Fig. 7(a)] are nonlinear for the bulk sample, the Arrot plot [Fig. 7(d)] gives zero value of M_S and confirms the paramagnetic state of bulk sample at 50 K. This is consistent with paramagnetic to ferrimagnetic transition temperature $T_C \sim 45$ K, observed from the $M(T)$. Hence, a nonlinear increase of $M(H)$ at 50 K (above T_C) can be attributed to the short range interactions among the spins or clusters of spins, as found in another system.[24] The upward curvature in Arrot plot, even in the order magnetic state, is not very conventional. The gradual increase of upward curvature with increase of temperature above T_C of the mh48 sample [Fig. 7(f)] suggests that the paramagnetic contribution or disorder effect causes such curvature in Arrot plot even in the ferrimagnetic state. The more curvature in nanoparticle samples in comparison with the bulk suggests more magnetic disorder for lower particle sample. The paramagnetic contribution from each isotherm at $T \leqslant T_C$ was determined by fitting the data above 10 kOe either to a linear equation (example 10 K data of bulk sample) or a nonlinear equation (example: 40 K data of bulk sample). We find that the value of the spontaneous magnetization (M_S), determined from the revised Arrot plot (not shown in figures), after the subtraction of the paramagnetic contribution is slightly higher than that obtained without subtracting the PM contribution. Figure 8 shows the temperature dependence of M_S for bulk and nanoparticle samples. We have observed that M_S is decreasing for lowering particle size and M_S is not zero above 45 K, as in bulk, for nanoparticles. By definition T_C, i.e., paramagnetic to ferrimagnetic transition temperature, is the temperature below which the nonzero value of M_S exists in the sample. Therefore Fig. 8 suggests the increase of T_C in the temperature range 45–55 K with the decrease of particle size. To confirm the increase of T_C, we have performed ac susceptibility measurements for selected samples and the data are shown in Fig. 9. The sharp transitions (peak) both in χ' (real part of ac susceptibility) and in χ'' (imaginary part of ac susceptibility) near T_C and T_S are observed [Figs. 9(a) and 9(b)] for bulk sample, but no such peak either at T_C or T_S in χ' is seen for nanoparticle samples. However, χ'' shows a sharp peak which is independent of frequencies [Fig. 9(d)] and corresponds to the T_C of the sample. The occurrence of this χ'' peak at higher temperature for smaller particle samples [Fig. 9(b)] confirms the increase of T_C with decreasing particle size of $MnCr_2O_4$. A small (but clear) change in χ'' near $T_S \sim 18$ K for our smallest particle size sample suggests that the signature of the noncollinear spin transition is still present

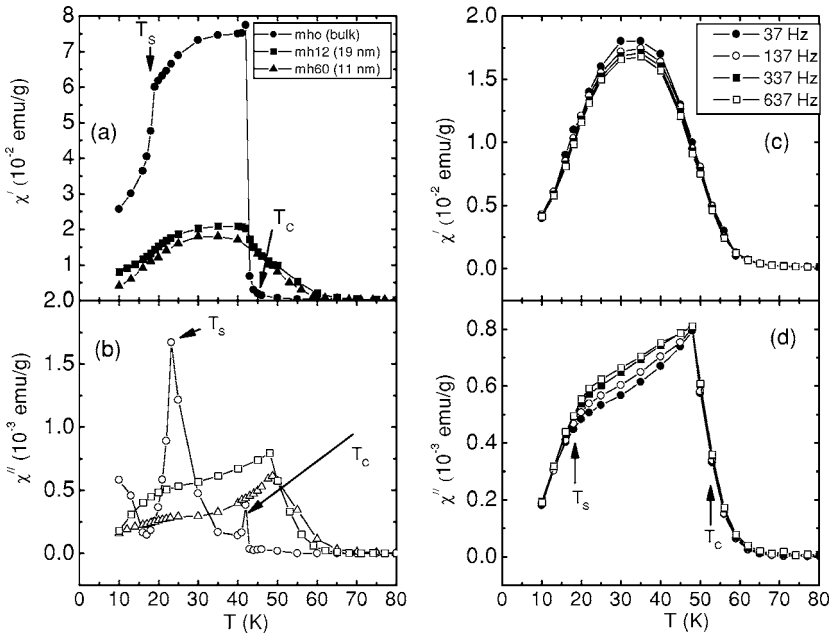

FIG. 9. Temperature dependence of real part (χ') and imaginary part (χ'') of ac susceptibility data at 1 Oe. (a) χ' for bulk, mh12, and mh60 at 37 Hz, and (b) corresponding open symbols χ'' data, (c) χ' at 37–637 Hz for mh60 (11 nm) sample, and (d) corresponding χ'' data.

there, but weak in magnitude. Although a broad maximum in χ', resembling superparamagnetic blocking, at about 35 K is noted for the mh60 sample, the other observations, i.e., almost no shift of χ' maximum with frequencies in the range 37–637 Hz [Fig. 9(c)] and no such maximum in χ'', suggest that such maximum in χ' is simply due to the disorder effect of shell spins, but not due to a typical superparamagnetic behavior. The presence of a sharp peak in χ'' near T_C suggests that long range ferrimagnetic order is still dominant in our smallest particle size (11 nm) sample, and coexists with the increasing disorder of shell spins.

III. DISCUSSION

It is interesting to note that $MnCr_2O_4$ nanoparticles show lattice expansion. A number of explanations for the lattice expansion in nanomaterials, such as change in oxygen coordination number with the cations,[13] change of valence state of cations,[25] crystallographic phase transformation,[26] and contribution of excess volume of grain boundary spins[27,28] are available in the literature. However, there is no satisfactory explanation. According to Banerjee *et al.*[27] lattice expansion in mechanical milled samples may be related to the mechanical strain induced effect, rather than intrinsic properties of the sample. This may not be true because lattice expansion has been observed in both mechanical milled nanoparticles as well as in chemical route prepared nanoparticles. The reported works did not show any correlation between the lattice expansion and magnetic order in nanoparticles. The present work clearly shows that magnetic order (spin structure) in $MnCr_2O_4$ is strongly dependent on the lattice parameter of the system. Details are discussed below.

The XRD pattern of our nanoparticle samples are identical with the bulk samples. The absence of any additional lines with respect to standard cubic spinel structure suggested that there is no crystallographic phase transformation in our nanoparticle sample. The agreement of the magnetic parameters (magnetic moment and T_C) of our bulk sample with literature value[6,9,14] has confirmed that Mn ions are in a divalent (Mn^{2+}: $3d^5$) state. The mechanical milling in argon atmosphere is also not in favor of the formation of Mn ions with higher ionic (3+ or 4+) states. We know that the outer shell spin configurations of Mn^{2+} (moment: 5 μ_B), Mn^{3+} (moment: 4 μ_B), and Mn^{4+} (moment: 3 μ_B) are $3d^5$, $3d^4$, and $3d^3$, respectively. If Mn^{3+} or Mn^{4+} exists in our nanoparticle samples, one would expect the decrease of lattice parameter with decrease of particle size. The increase of lattice parameter in nanoparticle samples suggests that there is no change in valence state of Mn ions. Hence the decrease of magnetic moment in nanoparticle samples may be consistent with the core-shell model.[18] The core-shell model[18] suggests that disorder in shell (surface) spins decreases the net magnetization of the ferrimagnetic nanoparticle and such contribution of shell spins increases on decreasing the size of particle. The question arises, whether shell spin disorder is responsible only for the decrease of magnetization or this disorder may be translated into the lattice dynamics which can show "disorder induced" magnetic order.[29] The role of shell (surface) spin disorder has been reported[23,30,31] in a different kind of nanoparticle spinel.

We now consider the effect of shell spin disorder in $MnCr_2O_4$ nanoparticles. The microstructure of the shell may influence the lattice expansion in two ways, by increasing the free excess volume of the incoherent shell spins in the interface structure, and by lowering symmetry in oxygen coordination numbers with surface cations. Fava *et al.*[13] have already shown that increase of lattice volume in $MnCr_2O_4$ is related to the change in oxygen coordination number with the cations. Consequently, the lattice pressure on core spins may be reduced by the elastic coupling between (shell and core) spin lattices.[27] Many other factors such as breaking of long range crystallographic coherent length and random orientations of shell spins may exhibit interatomic spacing (lattice parameter) which is different from bulk lattice. Experimental results show larger interatomic spacings (lattice parameter) in $MnCr_2O_4$ nanoparticle. Since the ratio of J_{AB} and J_{BB} superexchange interactions in chromites depends upon both the bond angle and bond length (interatomic spacings) of B site spins (cations),[6] any change in the spin configuration either in shell or core must be reflected in the magnetic properties of nanoparticles. If the lattice expansion in $MnCr_2O_4$ nanoparticles is intrinsic, one would expect two important effects. First, direct cation-cation (antiferromagnetic) interactions will be diluted. Consequently, noncollinear spin structure between B site Cr^{3+} cations of bulk $MnCr_2O_4$, revealed by the magnetic transition at $\sim$18 K,[6] will be decreased in $MnCr_2O_4$ nanoparticles. Second, intersublattice (J_{AB}) super-exchange (ferrimagnetic in nature) interactions will dominate over B-B (J_{BB}) interactions (antiferromagnetic in nature).[6,8] Consequently, increase of T_C is expected, as T_C is proportional to J_{AB} in spinel. A strong relationship between the lattice parameter and T_C of chromites has been found from the comparison of lattice parameters ($\sim$8.41, 10.18, and 10.23 Å, respectively) vs T_C ($\sim$45, 80, and 84.5 K, respectively) for bulk $MnCr_2O_4$, $MnCr_2S_4$, and $CdCr_2S_4$ with identical lattice (cubic spinel) structure. The enhancement of T_C in $MnCr_2O_4$ nanoparticles, therefore, suggests the increase of interatomic distance between B site (Cr-Cr) cations.

We now show that the enhancement of T_C is not due to the site exchange of Mn^{2+} and Cr^{3+} among A and B sites in nanoparticles. Both Rh and Cr atoms are highly stabilized in B sites of cubic spinel structure due to their strong affinity for B site. The work on mechanical milled $CoRh_2O_4$ nanoparticles[23] suggested that there is no migration of Rh atoms from B site to A site for particle size down to $\sim$16 nm. On the other hand, a very small amount of cations exchange among A and B sites in mechanical milled $Zn_{0.8}Co_{0.2}Fe_2O_4$ nanoparticles[30] has shown drastic enhancement of both magnetization and ferrimagnetic ordering temperature in comparison with their bulk sample. A schematic diagram (Fig. 10) shows that a similar type of enhancement in magnetization is also expected in $MnCr_2O_4$ nanoparticle, if mechanical milling really affects the site selection of cations (Mn^{2+} and Cr^{3+}). In bulk $MnCr_2O_4$ [Fig. 10(a)], A site is fully occupied by Mn^{2+} ions and B site is fully occupied by Cr^{3+} ions. Experimentally it has been found that magnetic moment of Mn^{2+} and Cr^{3+} ions are $\sim 5\mu_B$ and $3\mu_B$, respectively. For the sake of argument we assume [Fig. 10(b)] that a fraction (p of the Mn^{2+} ions migrate to B site in the exchange of equal

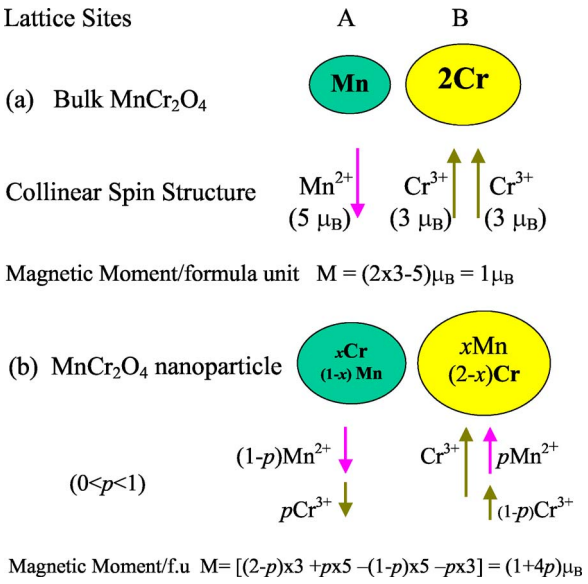

FIG. 10. (Color online) A schematic of cations distribution [Mn^{2+} (magenta color) and Cr^{3+} (olive color)] in A and B sites for collinear ferrimagnetic structure of $MnCr_2O_4$ bulk (a), and (b) nanoparticle with cations migration (assumed). P is the fraction of cations in bulk which can be exchanged between A and B sites in nanoparticle structure. The moments of cations in each (A or B) site are assumed to be parallel and moments of two sites are antiparallel to each other.

number of Cr^{3+} ions to the A site in $MnCr_2O_4$ nanoparticles. The enhancement of total magnetization was expected in $MnCr_2O_4$ nanoparticles by considering the formula for total magnetization of spinel oxide ($M=M_B-M_A$, where M_B and M_A are magnetization of B and A sites, respectively, and the number of B site magnetic ions is double in comparison with the number of A site magnetic ions). However, experimental results show the decrease of magnetization with decreasing particle size. Hence we exclude the possibility of the site exchange of Mn^{2+} and Cr^{3+} among A and B sites in $MnCr_2O_4$ nanoparticles. Therefore Cr atoms even in nanoparticle show the great affinity to occupy the B site alone, as in bulk.

We now consider the particle size effect on the magnetic transition at ~18 K. Neutron experiments[8,9] confirmed that collinear to noncollinear (canted) spin transition is the origin of magnetic transition at ~18 K in bulk $MnCr_2O_4$. Further the increase of surface spin canting should result in a more prominent magnetic transition at ~18 K, and decrease of ferrimagnetic ordering temperature (T_C) for nanoparticles. Our experiment on $MnCr_2O_4$ nanoparticles shows neither strong magnetic transition at 18 K nor decrease of T_C for smaller particles. On the other hand, experiment confirmed the enhancement of T_C in $MnCr_2O_4$ nanoparticles. Hence weakening of the magnetic transition at 18 K in nanoparticles is not due to the effect of increasing surface spin canting. This is an effect of intrinsic change in noncollinear to collinear spin structure in B sites of $MnCr_2O_4$ and directly correlated with lattice expansion of the system.[32]

The other observations of nanoparticles, i.e., (i) large magnetic irreversibility between MFC and MZFC, and (ii) appearance of a maximum in MZFC below 40 K, resemble superparamagnetic-like blocking of nanoparticles. But, ac susceptibility measurement shows no typical superparamagnetic behavior in our nanoparticles. Such behavior, in fact, arises due to the increasing disorder of surface spins. The $M(T)$ data, following Bloch law, near 44 K (close to T_C ~45 K of bulk sample) for all samples suggest that strong ferrimagnetic order of core spins (bulk) is almost retained. We therefore suggest that surface spin disorder in nanoparticles is translated into the lattice dynamics to cause a geometrical frustration effect[29] and results in lattice expansion.

IV. CONCLUSIONS

Bulk $MnCr_2O_4$ is a ferrimagnet with paramagnetic to collinear ferrimagnetic state at $T_C \approx 45$ K and collinear ferrimagnetic to noncollinear ferrimagnetic state below 18 K. Experimental results suggest that the noncollinear ferrimagnetic state in $MnCr_2O_4$ occurs due to direct interactions between B site Cr^{3+} ions. The B site direct interactions, represented by magnetic transition at 18 K, decreases in $MnCr_2O_4$ nanoparticles. We attribute the decrease of B site direct interactions to the lattice expansion in $MnCr_2O_4$ nanoparticles, essentially confined in shell, which results in the change from noncollinear to collinear structure of B site spins. Our experimental results are consistent with the proposal made by Wickham and Goodenough that direct (antiferromagnetic) interactions between B site cations are possible in chromites and causes collinear to noncollinear ferrimagnetic transition at about 18 K. Reduction of magnetic moment, large magnetic irreversibility between MZFC and MFC, and appearance of superparamagnetic-like blocking are some of the notable disorder effects in nanoparticles. The high value of Bloch exponent $\alpha=3.35$ for bulk $MnCr_2O_4$ and the decrease of α with decreasing particle size, identify unconventional magnetic features in $MnCr_2O_4$.

ACKNOWLEDGMENTS

We thank Chandan Mazumdar for useful discussions and SQUID measurements. We also thank Pulak Roy for TEM data.

*Present address: Department of Physics, Mahishadal Raj College, Mahishadal, East Midnapore, Pin Code: 721628, West Bengal, India. Electronic address: rnb@cmp.saha.ernet.in
†Electronic address: ranga@cmp.saha.ernet.in

[1] S. Krupika and P. Novak, in *Ferromagnetic Materials*, edited by E. P. Wolfarth (North-Holland, Amsterdam, 1982), Vol. 3, p. 189.
[2] J. L. Dormann and M. Nogues, J. Phys.: Condens. Matter **2**, 1223

(1990).
[3] A. P. Ramirez, R. J. Cava, and J. Krajewski, Nature (London) **386**, 156 (1997).
[4] M. S. Park, S. K. Kwon, and B. I. Min, Phys. Rev. B **64**, 100403(R) (2001).
[5] V. A. M. Brabers, Phys. Rev. Lett. **68**, 3113 (1992).
[6] D. G. Wickham and J. B. Goodenough, Phys. Rev. **115**, 1156 (1959).
[7] S.-H. Lee, C. Broholm, T. H. Kim, W. Ratcliff II, and S.-W. Cheong, Phys. Rev. Lett. **84**, 3718 (2000).
[8] V. Tsurkan, M. Mucksch, V. Fritsch, J. Hemberger, M. Klemm, S. Klimm, S. Korner, H.-A. Krug von Nidda, D. Samusi, E.-W. Scheidt, A. Loidl, S. Horn, and R. Tidecks, Phys. Rev. B **68**, 134434 (2003).
[9] J. M. Hasting and L. M. Corliss, Phys. Rev. **126**, 556 (1962).
[10] S. Radha, S. B. Roy, A. K. Nigam, and G. Chandra, Phys. Rev. B **50**, 6866 (1994).
[11] K. Tomiyasu, J. Fukunaga, and H. Suzuki, Phys. Rev. B **70**, 214434 (2004).
[12] T. W. Swaddle, J. H. Lipton,G. Guastalla, and P. Bayliss, Can. J. Chem. **49**, 2433 (1971).
[13] F. F. Fava, I. Baraille, A. Lichanot, C. Larrieu, and R. Dovesi, J. Phys.: Condens. Matter **9**, 10715 (1997).
[14] S. Horiuchi and S. Miyahara, J. Phys. Soc. Jpn. **28**, 529 (1970).
[15] Qi Chen and Z. J. Zhang, Appl. Phys. Lett. **73**, 3156 (1998).
[16] Z. Yang, S. Tan, Z. Chen, and Y. Zhang, Phys. Rev. B **62**, 13872 (2000).
[17] D. S. Williams, P. M. Shand, T. M. Pekarek, R. Skomski, V. Petkov, and D. L. Leslie-Pelecky, Phys. Rev. B **68**, 214404 (2003).
[18] R. H. Kodama, A. E. Berkowitz, E. J. McNiff, and S. Foner, Phys. Rev. Lett. **77**, 394 (1996).
[19] M. Lubecka, L. J. Maksymowicz, and R. Zuberek, Phys. Rev. B **42**, 3926 (1990).
[20] X. Battle and A. Labarta, J. Phys. D **35**, R15 (2002).
[21] P. V. Hendriksen, S. Linderoth, and P. A. Lindgard, Phys. Rev. B **48**, 7259 (1993).
[22] R. Abe, Y. Tsunoda, M. Nishi, and K. Kakurai, J. Phys.: Condens. Matter **10**, L79 (1998).
[23] R. N. Bhowmik, R. Nagarajan, and R. Ranganathan, Phys. Rev. B **69**, 054430 (2004).
[24] J. Mira, J. Rivas, M. Vazquez, J. M. Garcia-Beneytez, J. Arcas, R. D. Sanchez, and M. A. Senaris-Rodriguez, Phys. Rev. B **59**, 123 (1999).
[25] S. Tsunekawa, K. Ishikawa, Z.-Q. Li, Y. Kawazoe, and A. Kasuya, Phys. Rev. Lett. **85**, 3440 (2000).
[26] P. P. Chatterjee, S. K. Pabi, and I. Manna, J. Appl. Phys. **86**, 5912 (1999).
[27] R. Banerjee, E. A. Sperling, G. B. Thompson, H. L. Fraser, S. Bose, and P. Ayyub, Appl. Phys. Lett. **82**, 4250 (2003).
[28] L. Wang and F. S. Li, J. Magn. Magn. Mater. **223**, 233 (2001).
[29] S.-H. Lee, C. Broholm, W. Ratcliff, G. Gasparovic, Q. Huang, T. H. Kim, and S.-W. Cheong, Nature (London) **418**, 856 (2002).
[30] R. N. Bhowmik, R. Ranganathan, S. Sarkar, C. Bansal, and R. Nagarajan, Phys. Rev. B **68**, 134433 (2003).
[31] R. N. Bhowmik, R. Ranganathan, R. Nagarajan, Biswatosh Ghosh, and S. Kumar, Phys. Rev. B **72**, 094405 (2005).
[32] A. Fukunaga, S. Chu, and M. E. McHenry, J. Mater. Res. **13**, 2465 (1998).